Length-Selective Chemical Assembly of Vertically Aligned Carbon Nanotubes

Hussein, Zarrar; Rawson, Frankie J.; Goldberg Oppenheimer, Pola; Acton, Aaron; Mendes, Paula M.

DOI:
10.1002/admi.201500860
10.1002/admi.201500860

Document Version
Publisher's PDF, also known as Version of record

Citation for published version (Harvard):
Hussein, Z, Rawson, FJ, Goldberg Oppenheimer, P, Acton, A & Mendes, PM 2016, 'Length-Selective Chemical Assembly of Vertically Aligned Carbon Nanotubes', *Advanced Materials Interfaces*, vol. 3, no. 11. https://doi.org/10.1002/admi.201500860, https://doi.org/10.1002/admi.201500860

ADVANCED MATERIALS INTERFACES
www.advmatinterfaces.de

Length-Selective Chemical Assembly of Vertically Aligned Carbon Nanotubes

*Zarrar Hussein, Frankie J. Rawson, Pola G. Oppenheimer, Aaron Acton, and Paula M. Mendes**

Many potential applications of carbon nanotubes (CNTs), ranging from electronics and optoelectronics to biology and medicine, require length-controlled and well-aligned CNTs on surfaces. In this work, the length selectivity behavior of wet-dispersed CNTs on gold functionalized surfaces is investigated, providing new mechanistic insights into the length-selective process that occurs upon chemical assembly. A combination of experimental evidence derived from atomic force microscopy and plane and cross-sectional transmission electron microscopy implies a length-selective deposition of CNTs on the functionalized gold surface. All the solutions containing either a high distribution of longer or shorter CNTs lead to the selective formation of vertically aligned carbon nanotubes with average lengths of 10.6 ± 3.1 nm. It is postulated that such length-selective phenomenon is not only driven by diffusion mechanisms but also is governed by the interactions between the CNTs and the chemically functionalized surfaces. The orientation of the initial attached nanotubes, which act as nucleation sites in the CNT assembly process, is proposed to dictate the CNT length distribution on the surface and be dependent on the packing and ordering of the molecules on the functionalized surface.

1. Introduction

Vertically aligned carbon nanotubes (VACNTs) have attracted significant recent attention due to their wide-ranging applications from electronics and optoelectronics through to biology and medicine.[1–4] Owing to their 3D highly oriented structures and remarkable physical and chemical properties, VACNTs are currently regarded as superior materials for field emitters[5] and optoelectronic devices[3] as well as highly sensitive platforms for chemical and biological sensing.[6,7] With such applications in mind, VACNTs have been successfully prepared using either direct growth by chemical vapor deposition[5,8] or chemical assembly of resynthesized CNTs.[9,10] The chemical assembly route taken to vertically align CNTs is more cost-effective and allows for greater flexibility in selecting the CNT–substrate interactions and the substrate used. In this regard, vertical self-assembly of CNTs have been achieved on different substrates, including ITO, gold, silver, silicon, glass and Nafion films, through metal-assisted chelation,[11] electrostatic interactions,[12] π–π interactions,[13] and different covalent bonds.[2,14–18]

A key issue for chemical assembly of VACNTs is to gain a full understanding and control over the assembly behavior since the properties of the VACNTs are intimately related with, among others, their assembly density, location, average length, and length distribution on the substrate.[10,14,15] For example, advantages in electrical behavior of the unselective vertical alignment of random geometries of CNTs, over random dispersed CNTs on conducting surfaces, has been established.[15] However, to the best of our knowledge no finite control length and/or orientation of alignment of chemically assembled CNTs has been presented.

CNT density studies have demonstrated that CNT surface coverage is a time-dependent process with two distinctive kinetic stages: one fast stage that can last from 2 to 4 h depending on the assembly approach, followed by a relatively slow stage that can take up to 10 h or longer.[11,14,16,19] Research work has been also devoted to the site-selective assembly of vertically aligned CNTs on patterned surfaces, which have been achieved through different lithographic techniques, such as microcontact printing,[20] photolithography,[21] and electron-beam lithography.[22] However, while CNT density and spatial positioning can be achieved with relative ease, understanding and controlling the average length and length distribution of the standing CNTs via chemical assembly remains elusive. The formation of VACNTs via chemical assembly relies on the use of shortened CNTs with a broad length distribution ranging from a few to hundreds of nanometers. Previous investigations have revealed that such uneven distribution is partially reflected in the corresponding VACNT-functionalized surfaces.[16,17,19] Along this line, Yu et al.[17] for example, reported aligned CNTs formed by self-assembly on a silicon surface using shortened CNTs having an average length of 380 nm and a maximum

Z. Hussein, Dr. P. G. Oppenheimer, Dr. A. Acton, Prof. P. M. Mendes
School of Chemical Engineering
University of Birmingham
Edgbaston, Birmingham B15 2TT, UK
E-mail: p.m.mendes@bham.ac.uk
Dr. F. J. Rawson
Laboratory of Biophysics & Surface Analysis
School of Pharmacy
University of Nottingham
University Park
Nottingham NG7 2RD, UK

The copyright line of this paper was changed 6 June 2016 after initial publication.

DOI: 10.1002/admi.201500860

length of about 850 nm. The average and maximum lengths of the CNTs on the surface were shown to progressively increase with surface reaction time, of which were 3 nm and 28 nm, respectively, for 4 h reaction and 65 nm and 204 nm, respectively, for a 48 hour reaction. As in other studies,[16,19] the heights observed for the protruding nanotubes were considerably shorter than the known distribution of lengths of the cut nanotubes. These studies underpin unresolved issues regarding the length-selective process that occurs upon chemical assembly including, which parameters can influence the length selectivity pattern, to which extent the solution length distribution can affect the surface and, ultimately, can such selective process lead to a very narrow length distribution of aligned CNTs on surfaces. Only by addressing these aforementioned issues can chemical assembly-based VACNT technology move forward, expand their functionality and performance and ultimately realize their true potential.

For these reasons, we set out to investigate the length selectivity behavior of dispersed CNTs on gold-functionalized surfaces. The approach we have taken is to assess how different length distribution regimes can alter the length selection pattern on the surface. To assemble the CNTs on the gold surface, a 4-aminothiophenol (ATP) self-assembled monolayer (SAM) was prepared on gold, which can then be used to orchestrate the immobilization of shortened CNTs. Pristine single-walled CNTs were shortened by sonication-assisted oxidative cutting to obtain open-ended nanotubes with terminal carboxylic acid groups.[23] Different cutting times were employed (4–10 h) in order to generate CNTs with different length distributions. The assembly was based on the condensation reaction between the carboxylic acid moieties of the CNTs and the amino groups on the SAM surface.

2. Results and Discussion

The formation of the ATP SAM on gold was studied by means of ellipsometry and contact angle. The clean bare gold substrates displayed low H_2O advancing (θ_{Adv}) and receding (θ_{Rec}) contact angles (22 ± 1° and 16 ± 1°, respectively), which increased to 72 ± 1° and 63 ± 1°, respectively, after 24 h SAM formation. Note that the hysteresis (θ_{Adv}–θ_{Rec}) value of 9° suggests the presence of a well-ordered monolayer. Ellipsometry revealed that the average film thickness was 0.45 ± 0.05 nm, which is less than the theoretical molecular length of the molecules (0.7 nm). The discrepancy between molecular length and SAM thickness is ascribed to the tilt angle of the SAM molecules.[24,25]

Pristine single-walled CNTs purchased from NanoLab (USA) were grown via chemical vapor deposition yielding CNTs between 1 and 5 µm in length with an approximate diameter of 1.4 nm. They were cut by being exposed to ultrasonication and simultaneous oxidative acid treatment and we investigated the cutting procedure applied at varying times (from 4 to 10 h). Consistent with previous studies,[23,26] the length of the shortened CNTs varies as a function of cutting time, wherein a high percentage of shorter nanotubes can be achieved by increasing the CNT cutting time. In order to determine the average degree of CNT length distribution following the cutting procedure, we have performed a quantitative analysis of the transition electron microscopy (TEM) images (**Figure 1**a–h). While for each cutting time, the samples were polydispersed, 23 ± 5% of the CNTs were in the range of 500–600 nm (Figure 1a,b), 20 ± 3% were in the range of 250–300 nm (Figure 1c,d), 21 ± 5% fell in the range between 120 and 150 nm (Figure 1e,f) and 23 ± 2% were found in the range of 60–90 nm (Figure 1g,h), with it representing the majority of the CNTs population in each case. The longest CNTs present in each sample post-sonication also followed similar patterns, with 4, 6, 8, and 10 h of cutting times resulting in maximum lengths of 700, 500, 250, and 210 nm, respectively.

The assembly of the CNTs was achieved by immersing the ATP SAM surfaces for 16 h on the different CNT suspensions with dicyclohexylcarbodiimide (DCC) as a coupling agent. Based on previous research work,[14,16,19] this time of incubation (16 h) was selected to ensure higher packing density and coverage of the CNTs on the ATP SAM-modified gold surface. Atomic force microscopy (AFM) was used to probe the morphology of the surfaces before and after CNTs assembly. In contrast, with a smooth flat ATP SAM surface, closely packed needle-like protrusions were clearly observed for the different CNT cutting times (**Figure 2**). Surprisingly, there was no trend toward variations of CNT length distributions on the surfaces with decreasing cutting time. The distribution of lengths on the surface, obtained from the mean height roughness, for each treatment time was very similar, 10.8 ± 3.0, 10.4 ± 3.2, 10.5 ± 3.4, 10.7 ± 3.0 nm for 4, 6, 8, and 10 h, respectively, with the majority of the nanotubes being between 5 and 10 nm in height. For comparison, control surfaces, i.e., i) clean gold surfaces and gold surfaces ii) without ATP SAM and exposed to CNTs with DCC as a coupling agent and iii) with ATP SAM and exposed to CNTs without DCC as coupling agent, were also analyzed by AFM (Figure S1, Supporting Information). All the control surfaces were essentially smooth and featureless as observed for the AFM images of the ATP SAM (Figure 2a).

The maximum lengths of the protrusions for the different CNT cutting times were about 20 nm (Figure 2b–e), which were significantly shorter than that of the suspension forms. The surface roughness for the ATP SAM was determined by AFM to be 0.99 ± 0.01 nm, which increased upon CNT assembly but largely unchanged for the different CNT cutting times (2.33 ± 0.05, 2.66 ± 0.16, 2.36 ± 0.14, and 2.26 ± 0.03 nm for 4, 6, 8, and 10 h cutting time, respectively). These findings further indicate similar morphological characteristics among the modified gold substrates with VACNTs. The apparent widths of the needle-like protrusions (from the AFM images, Figure 2) are about tens of nanometers, which are significantly larger than the diameter of the single CNTs. This difference is believed to arise from CNTs aggregation in the assembly process due to the strong van der Waals interactions between the sidewalls of the nanotubes.

Another feature to note in the AFM images is that all CNTs are vertically aligned and not lying horizontally on the substrate. This element of orientation control is attributed to a high concentration of carboxyl groups on the severed edges of the CNTs, allowing a high number of amide bonds to be formed between each nanotube and the ATP SAM on the gold surface. The preferred vertical conformation of the CNTs on the surface can also be explained by the hydrophilic nature of the amino-terminated gold substrate that makes interactions with

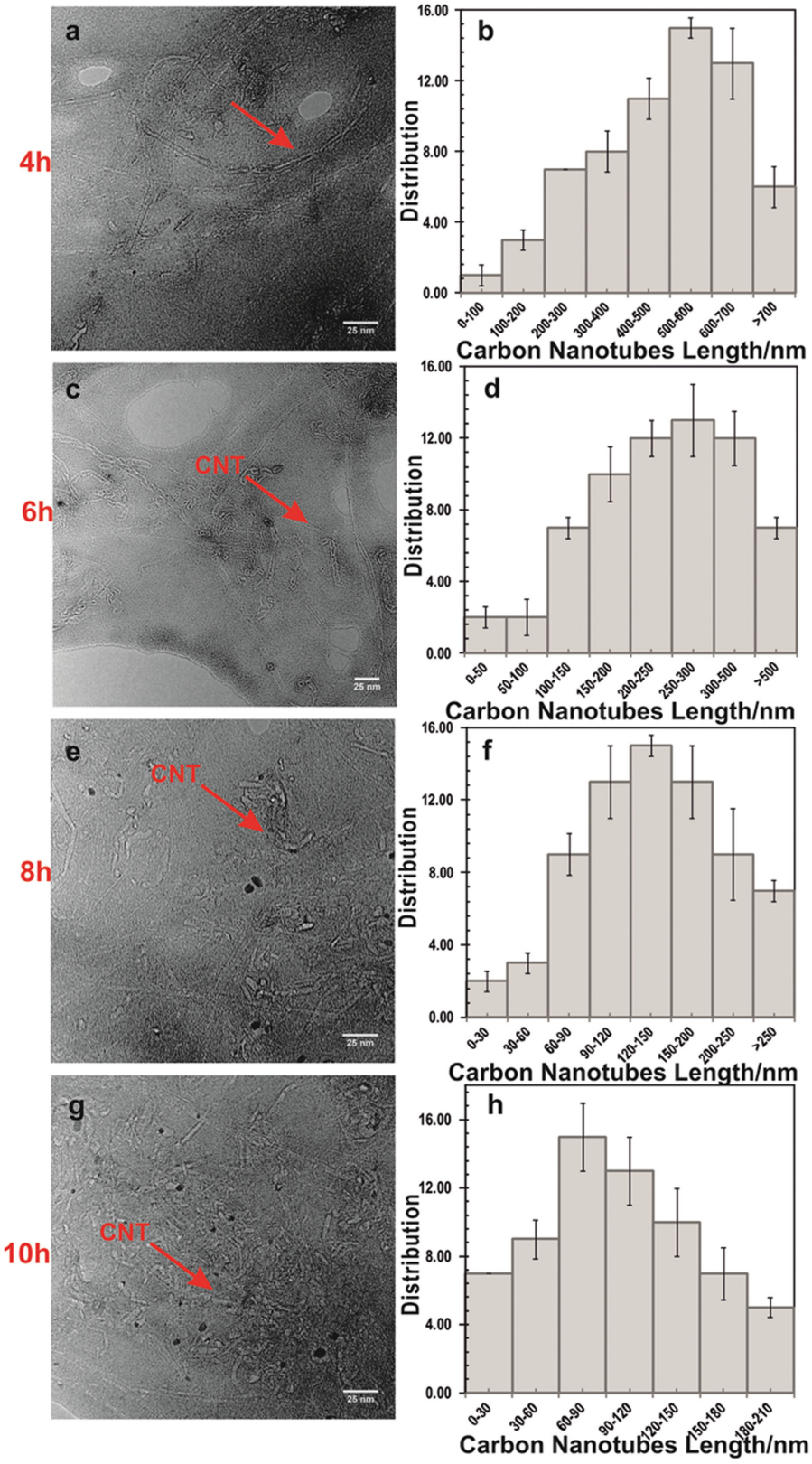

Figure 1. Representative a,c,e,g) TEM images of the dispersed CNTs as function of the cutting times ranging from 4 to 10 h. The arrows indicate the CNTs. The b,d,f,h) histograms show the distribution of the CNTs lengths as function of the various cutting times as extracted from TEM images (n = 18 micrographs).

the hydrophobic sidewalls of the nanotubes very unfavorable.

A microtomed cross section examined by TEM yields additional insight into the CNTs orientation and lengths attached to the surface. **Figure 3** reveals that the CNTs are vertically assembled on the ATP SAM surface with nanotube lengths in good agreement with those measured by AFM. Shorter (4 h) and longer cutting times (10 h) yielded average VACNT lengths of 10.5 ± 0.4 nm and 10.9 ± 0.6 nm, respectively.

Electrochemical studies provided additional evidence of surface functionalization and homogeneity of the different VACNT-functionalized surfaces. **Figure 4** shows cyclic voltammograms (CVs) obtained in the presence of 1×10^{-3} M solution of ferricyanide at unmodified gold, surface functionalized with the ATP SAM and modified ATP SAM with CNTs derived from the different cutting time points. In CVs obtained at gold (Figure 4a), a redox couple was observed associated with the Fe^{2+}/Fe^{3+} and was characterized by a mean anodic peak potential (Figure 4a Inset) of 0.346 ± 0.014 V and a cathodic peak potential of 0.02 V. When CVs were obtained at surfaces modified with ATP SAM, an anodic peak potential of 0.488 ± 0.022 V was obtained and a mean cathodic peak potential of –0.028 ± 0.041 V. The peak separation measured from CVs logged at ATP-modified surfaces yielded a peak separation of 0.516 V versus 0.326 V obtained from CVs generated at unmodified gold, which indicates sluggish electron transfer and is consistent with the blocking nature of ATP films previously reported on gold.[27] If we compare the peak potentials obtained from CVs generated at the gold-modified ATP SAM surface to peak potentials obtained from CVs logged using surfaces functionalized with VACNTs (Figure 4b inset) exposed to acid treatment for varying times of 4, 6, 8, and 10 h, mean peak separation values of 0.168, 0.172, 0.164, 0.170 V were obtained, respectively. The significant difference between peak separation in CVs logged using ATP modified gold and those functionalized with CNTs arises from the fact that the ATP monolayer slows the

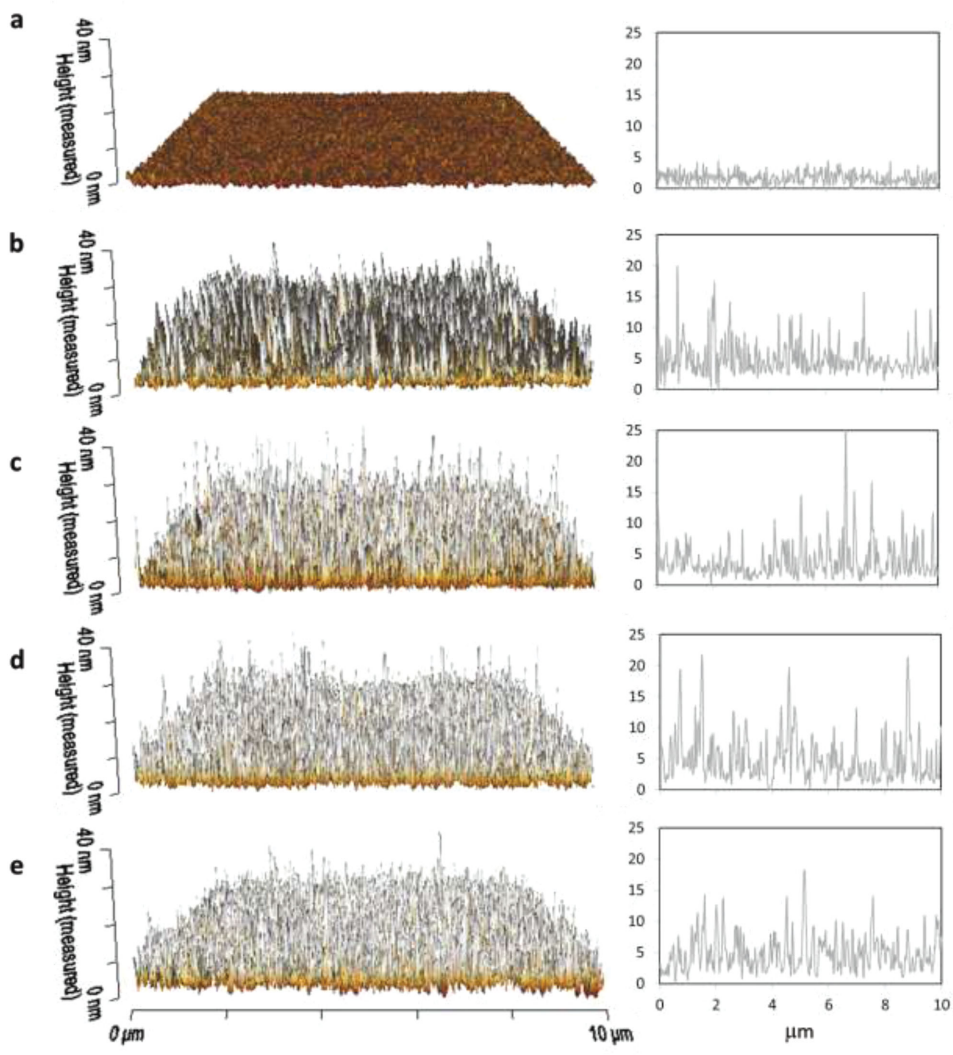

Figure 2. Representative tapping mode AFM images and height profiles of gold surfaces modified with a) ATP SAM and ATP SAM with CNTs derived from the different cutting time points: b) 4 h, c) 6 h, d) 8 h, and e) 10 h.

electron transfer process and this behavior has previously been observed.[27] We can rule out that the difference observed in the cyclic voltammetric behavior between ATP-modified surfaces and those further modified with CNTs is due to ohmic drop for a number of reasons. First, the positioning of the electrodes was consistent between experiments due to the cell design. We used a relatively slow sweep rate of 100 mV s^{-1}. Moreover, if cyclic voltammetry is performed at a relatively fast sweep rate there is a current transient due to the charging and discharging of the electrochemical double layer, which is displayed in the cyclic voltammograms, by a lagging in the true potential, and therefore the peak separation becomes larger. In particular, when the electrodes area is larger the contribution of this transient from charging the double layer increases and therefore an even bigger shift in increased peak separation would be observed. Therefore, we learn from AFM data that the electrode area becomes more-rough and consequently the charge associated with the

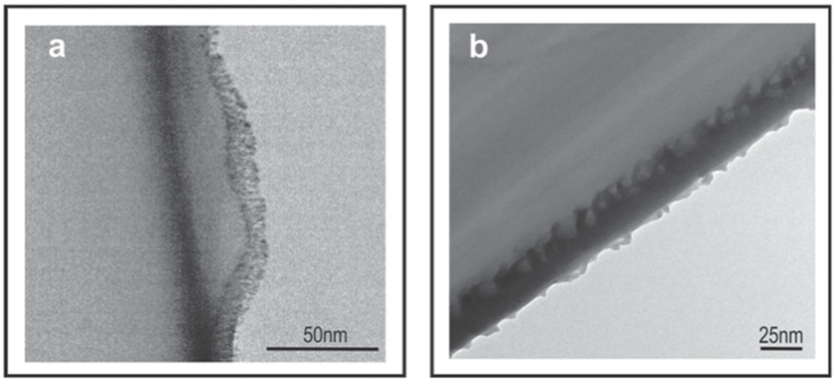

Figure 3. Cross-sectional TEM micrographs of VACNTs organization on the ATP SAMs on gold substrates after cutting for a) 4 and 10 h.

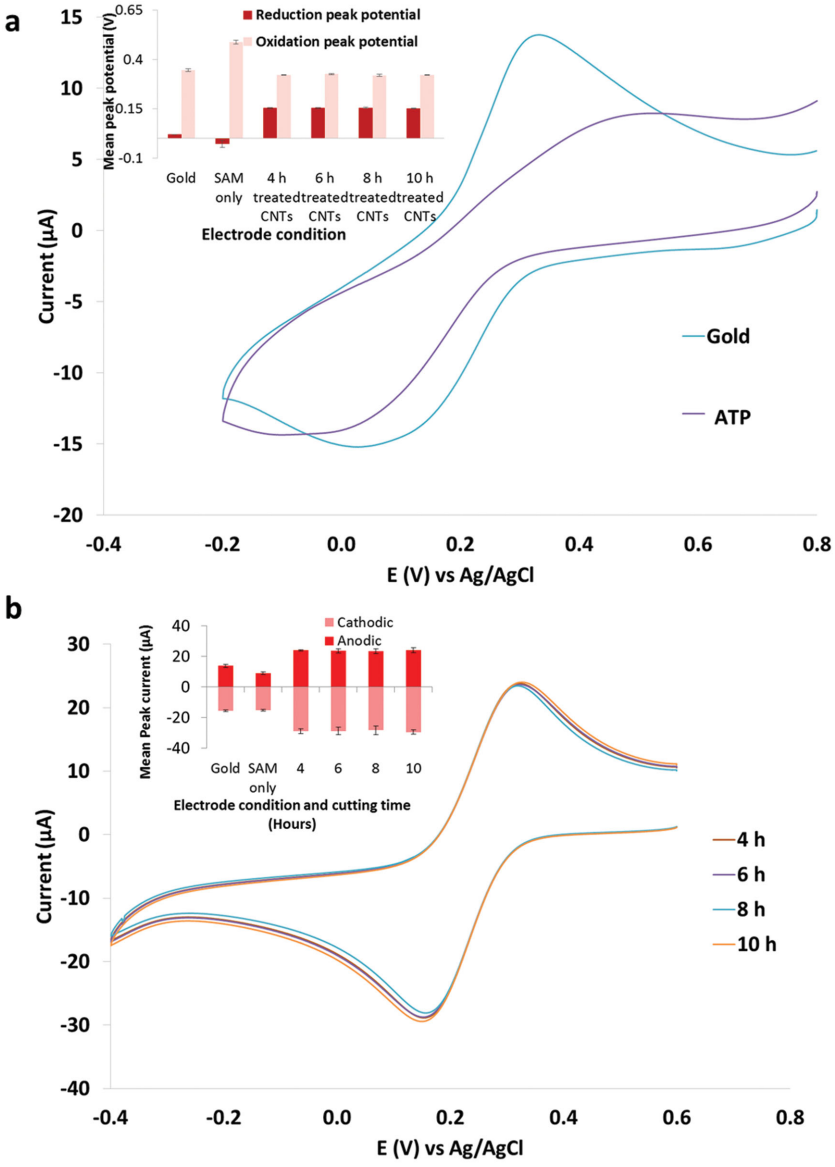

Figure 4. a) Mean CV ($n = 5$) obtained for solutions of 1×10^{-3} M ferricyanide in 50×10^{-3} M phosphate buffered saline (PBS) at bare gold, gold electrodes modified with SAMs formed with ATP. Insets are the mean peak potentials obtained from CV in Figure a for bare gold, gold modified with ATP SAM and working electrodes modified with acid treated CNTs at varying times of 4, 6, 8, and 10 h obtained from means CVs in Figure b. b) Mean CVs ($n = 5$) obtained for solutions of 1×10^{-3} M ferricyanide in 50×10^{-3} M PBS at working electrodes modified with acid treated CNTs at varying times of 4, 6, 8, and 10 h at a scan rate of 100 mV s^{-1}. Inset represents the measured mean peak cathodic and anodic currents at bare gold, ATP modified and surfaces modified with the CNTs exposed to acid for varying times. Error bars represent ±1 standard deviation of the mean.

setting up of the double layer would be greater. Consequently, it would be expected if ohmic loss was the reason for the change in behavior then the peak separation for cyclic voltammograms generated at CNTs surfaces would be large than when compared to the ATP-modified surface. On the contrary, this was not the case, and therefore all of the above indicates the difference in peak potentials arises from electron transfer rate differences between the surfaces. The magnitude of the peak current obtained for an electrochemical reversible (1) and for an irreversible (2) process in a CV is defined by the Randles–Sevcik equation:

$$i_p = (269000)\, n^{3/2} A C D^{1/2} \upsilon^{1/2} \quad (1)$$

$$i_p = (299000)\, n(\alpha n_a)^{1/2} A C D^{1/2}\, \upsilon^{1/2} \quad (2)$$

where i_p is current (A), n is the number of electrons involved in the charge transfer step, α is the transfer coefficient, n_a is the number of electrons involved in the charge-transfer step, A is the electroactive area (cm^2), D is the diffusion coefficient of species of interest (cm^2 s^{-1}) (in this case, ferricyanide), and C is the bulk concentration of ferricyanide (mol cm^{-3}).

Thus, it would be envisaged that if there was a correlation between acid treatment and population differences in heights of CNTs that tethered to the surfaces, then the electrochemical active area would be different between samples prepared with the CNTs cut with acid at varying times. If this was the case, it would be expected that we would observe CVs with significantly different magnitudes in peak current as defined by the Randles–Sevcik equations due the electrochemical active area differing. On the contrary, from Figure 4b (Inset), which shows a plot of mean peak current versus time at which the CNTs were acid treated prior to coupling, the peak currents observed were not significantly different. This lack of difference in the magnitude of the peak current obtained indicates that the electrochemically active area was approximately the same between the surfaces grafted with CNTs that were treated with acid at varying times. These results support the findings that the population of VACNTs, in terms of height that attaches to the SAM, is no different when compared to the cutting times.

Some features of these VACNTs provide information about their assembly behavior. The length distribution of the VACNTs is independent of the CNT length distributions under which the chemical assembly was performed. The studies also established that it was favorable for the short (5–10 nm) CNTs to assemble on the ATP SAM selectively to the longer (i.e., >20 nm) CNTs. These findings provide evidence that the chemical assembly process is dependent on the diffusional characteristics of the CNTs. Previous studies on the motional dynamics of CNTs have demonstrated that they undergo both translation and rotation motion in solution,[28,29] allowing them to be redistributed in space and over various orientations. Since a CNT can be defined as a prolate ellipsoid,[30] the dependence of the

translational (D_{trans}) and rotational (D_{rot}) diffusion coefficients on carbon nanotube length can be described by the Stokes–Einstein relation:[31]

$$D_{trans} = \frac{k_B T}{6\pi\eta a} G(p)$$

and the Stokes–Einstein–Debye relation:

$$D_{rot} = \frac{k_B T}{8\pi\eta a^3} \left(G(p)\right)^3$$

In these relations, T is the temperature, η is the solution viscosity, k_B is the Boltzmann constant, a is the nanotube radius and $G(p)$ a function that depends only on the axial ratio (half-length (b)/ radius (a)) of the nanotube:

$$G(p) = \left(p^2 - 1\right)^{-1/2} \ln\left(p + \left(p^2 - 1\right)^{1/2}\right)$$

With a mean nanotube diameter of about 1.4 nm, $G(p)$ assumes values of 0.38 and 0.07 for a nanotube length of 10 and 100 nm, respectively. Thus, 100 nm nanotubes exhibit a translational diffusion five times slower than 10 nm nanotubes, implying a sluggish diffusion rate for the longest CNTs. The rotational motion is even more sensitive to changes in nanotube length than the translational motion. Rotational diffusion is about 150 times faster for 10 than 100 nm, allowing for the shortest nanotubes to be more easily oriented for vertical assembly on the surface. Following the above considerations, the diffusion-controlled transport mechanism to the surface can thus introduce a screening length, wherein the shortest carbon nanotubes are selected to be incorporated onto the surface.

Bearing in mind the diffusion-controlled transport of the CNTs that preferentially deliver the shorter CNTs to the surface of interest, a possible mechanisms is likely to lie at the origin of the observed vertical CNTs orientation with the selective lengths of 10.6 ± 3.1 nm: Highly uniform ATP SAM acting as nucleation sites for the shorter CNTs, yielding the ultimate packing conformation of the VACNTs. While the ATP-terminated surface on gold has led to a narrow distribution of CNTs of about 10 nm, previous work by Gooding and co-workers[15] using a different amine thiol—mercaptoethylamine—has resulted in tethered CNTs with length distributions in the hundreds of nanometers. Additionally, our previous work[2] utilizing an electrografted arylamine onto indium tin oxide has produced surfaces with a variety of lengths ranging from 10 to 60 nm. Similar lengths and length distribution to the latter have been observed for electrografted arylamine onto a pyrolyzed photoresist film.[16] This difference in length-selective capabilities cannot be explained based on the reactivity of the amino groups. ATP comprises an aromatic amine, conjugation of the amine lone pair with the aromatic group reduces the nucleophilicty of the amine and hence ATP is less reactive toward amide formation compared to an aliphatic amine such as mercaptoethylamine. If reactivity was a key factor on the selectivity, the mercaptoethylamine would have reacted faster with the shortest CNTs (first to reach the surface) and led to these surfaces displaying selectivity for the shortest CNTs. Also, if reaction kinetics was to play a major role in such process, both ATP surfaces and electrografted amino-terminated surfaces would have presented similar length trends—both contain aromatic amino groups. Since this is not the case, other factors should be considered such that the chemical assembly process depends sensitively on the details of the molecular interactions between the CNTs and the substrate surface. Most notably, the orientation and arrangement of the molecules on the surface appears to account for the differences in length control. ATP SAM provides better close-packing and well-ordered layer structures when compared to electrografted amino-terminated surfaces since the latter grow as a multilayer structure on the surface.[2] Based on the calculations above, the shortest nanotubes are the ones to reach the surface first and due to the highest rotational diffusion rate have the highest probability to react with the surface. It is reasonable to postulate that the presentation of the amino groups in a defined density and orientation allows the shortest functionalized carbon nanotube carboxylic acids to bind to several nearby amino groups, form amide bonds and align perpendicular to the surface (**Figure 5**a). Other amino-terminated surfaces might prevent the nanotube carboxylic acids from interacting with the required amino groups in an optimal fashion, so nanotubes can adopt different upright orientations (Figure 5b). These initial nanotubes act as "nucleation" sites for subsequent tubes to bond to the surface.[17] That is, once a nanotube is coupled to the surface, subsequent nanotubes rearrange themselves to allow high degrees of van der Waals interactions with the tethered nanotubes. The presence of only the shortest nanotubes on the ATP surfaces can plausibly be attributed to the restricted, specific conformations that the newcomers need to adopt to maximize van der Waals contacts and align perpendicular to the surface. The shortest nanotubes are expected to more easily take such specific conformations due to their high rotational diffusion rates and limited steric hindrance from the tethered CNTs. We postulate that nucleation sites with nanotubes exhibiting a degree of tilting allow for more flexible nanotube lengths to interact with the tethered CNTs.

3. Conclusion

In summary, we investigated the relationship between the lengths of single-walled carbon nanotubes (CNTs) chemically assembled on gold surfaces, and CNT lengths of solutions from which they were formed and did not observe any obvious correlation. Furthermore, relative to previous research work, our standing CNTs had smaller heights and a narrower length distribution. The ATP SAM is shown to be a very useful surface system for controlling the assembly of very short CNTs. Based on the present and previous findings, we hypothesized that the length-selective process is not only driven by the diffusion mechanisms but also governed by the interactions between the CNTs and the chemically functionalized surfaces. These studies are the initial and necessary steps towards a better understanding of the length-selective process that occurs upon chemical assembly. Furthermore, this work opens up the possibility of using substrate interfaces with tailored properties to create CNTs of uniform lengths on surfaces. This should ensure the

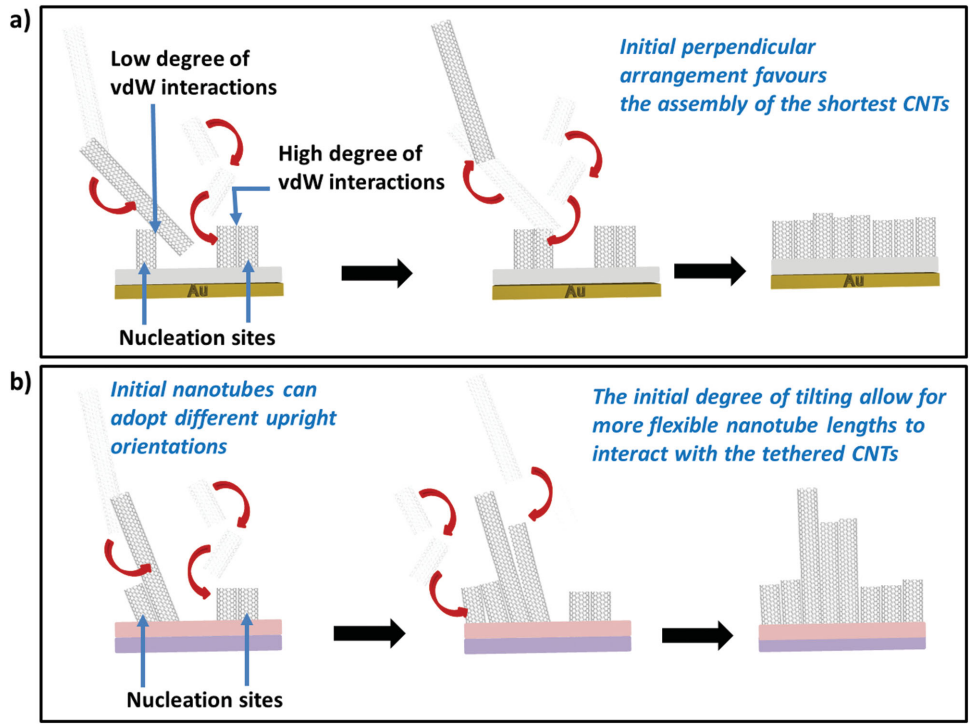

Figure 5. Schematic showing the dynamic process involved in the chemical assembly of CNTs as postulated to occur when initial nanotubes, which act as nucleation sites, are arranged a) perpendicular (ATP SAM) or b) tilted on the substrate surface.

chemical assembly route for functionalizing surfaces with VACNTs can now match and offer more suitable surfaces depending on the application than CVD CNT-functionalized surfaces. Importantly, this will provide a much high resolution in terms of nanoscale control of short vertically aligned CNTs which, we envisage will open up the technology to a plethora of applications from biosensing to electronics through to actuating surfaces.

4. Experimental Section

Chemicals and Materials: Commercially available chemicals and solvents were purchased from Aldrich Chemicals and Fisher Chemicals and were used as received. The single-walled carbon nanotubes were obtained from NanoLab Inc., with a diameter of ≈1.4 nm, length of 1–5 μm, purity of >95% and surface area of 1020.48 $m^2\ g^{-1}$. Polycrystalline gold substrates were purchased from George Albert PVD, Germany and consisted either of a 50 nm gold layer deposited onto glass covered with a thin layer of chromium as the adhesion layer (used for contact angle) or 100 nm gold layer on 100-4 in. silicon wafer, precoated with titanium as the adhesion layer (for ellipsometry analysis).

Preparation of Self-Assembled Monolayers: The Au substrates were cleaned by immersion in piranha solution (3:1, H_2SO_4 : 30% H_2O_2) at room temperature for 10 min, rinsing with ultra high pure (UHP) H_2O and then HPLC-grade EtOH thoroughly for 1 min. (*Caution: Piranha solution reacts violently with all organic compounds and should be handled with care*). Subsequently, the clean Au substrates were immersed in 1×10^{-3} M ethanolic solutions of 4-aminothiophenol to form the SAMs on the Au surfaces. After the desired immersion time, Au substrates were removed from the SAM solution and rinsed with HPLC EtOH.

CNT Cutting Procedure: CNT cutting was carried out by sonication in a mixture of sulfuric and nitric acids. Pristine (uncut) CNTs (25 mg) were added to 27 mL of a 3:1 mixture of concentrated H_2SO_4 and HNO_3 for the selected time points of 4, 6, 8, and 10 h. Following sonication, the contents were poured into 500 mL of distilled water and left to settle overnight. The CNTs were then filtered through a 0.22 μm hydrophilic PVDF filter (Millipore) under vacuum suction, with washing until the rinse water was close to pH 7. The filters containing the mats of CNTs were oven dried at 65 °C overnight. Suspensions of cut CNTs were prepared by sonication of dried CNTs mats in dimethyl sulfoxide (DMSO), making up stocks of 2 mg mL^{-1} solutions.

CNT Coupling and Assembly to the SAM on Gold: CNTs were coupled to the 4-aminothiophenol-modified gold surfaces by submerging the modified gold surfaces in a 0.2 mg mL^{-1} DMSO suspension of cut CNTs containing 0.5 mg mL^{-1} of dicyclohexylcarbodiimide (DCC). The reactants were sonicated for 30 min and then left for 16 h at room temperature. The resulting CNTs modified gold surfaces were sonicated for 5 min in acetone and 10 s in isopropyl alcohol. The surfaces were dried with argon gas between each washing step.

Contact Angle: Contact angles were determined using a home-built contact angle apparatus, equipped with a charged coupled device (CCD) KP-M1E/K camera (Hitachi) that was attached to a personal computer for video capture. The dynamic contact angles were recorded as a microsyringe was used to quasi-statically add water to or remove water from the drop. The drop was shown as a live video image on the PC screen and the acquisition rate was 10 frames per second. FTA Video Analysis software v1.96 (First Ten Angstroms) was used for the analysis of the contact angle of a droplet of UHP H_2O at the three-phase intersection. The averages and standard deviation of contact angles were determined from five different measurements made for each SAM.

Ellipsometry: The thickness of the deposited monolayers was determined by spectroscopic ellipsometry. A Jobin-Yvon UVISEL ellipsometer with a xenon light source was used for the measurements. The angle of incidence was fixed at 70°. A wavelength range of 280–820 nm was used. The DeltaPsi software was employed to determine the thickness values and the calculations were based on a three-phase ambient/SAM/Au model, in which the SAM was assumed to be isotropic and assigned a refractive index of 1.50. The thickness

reported is the average of five measurements, with the errors reported as standard deviation.

Atomic Force Microscopy: AFM images were recorded using the Nanowizard II atomic force microscope (JPK instruments, Germany), operating in tapping mode. CSC17 silicon cantilevers were employed, exhibiting ≈10 nm diameter pyramidal tips (MikroMasch, Tallinn, Estonia). An area of 10 µm x 10 µm was scanned. Five surface roughness measurements (R_a) were made per sample on five samples, including the control substrates. Since the VACNTs exhibit local differences in height, it can be denoted as CNTs having a (local) rough surface. Here the mean height roughness was used, which is defined as the difference in height between the average of *n* highest CNTs and *n* lowest valleys, in the evaluation profile/surface,[32–34] where *n* is the number of sampling points along the assessment length, which is 50 in this study. The errors reported are the standard deviation.

Transmission Electron Microscopy: Dispersed solutions of carbon nanotubes, which were exposed to different cutting times, were deposited on Cu grids with carbon coating on one side. The dispersion of the CNTs was carried out in cetyl trimethyl ammonium bromide (CTAB) (1%) and then centrifuged at 16 000 rpm to remove excess and clumped CNTs. This centrifuging method was repeated five times for each sample. For TEM cross-sectional imaging, the gold covered substrates with CNTs (4 and 10 h) were embedded into a Spurr epoxy resin (either top or bottom side). The substrates were subsequently removed and the films were sectioned using a diamond knife in a Leica Ultracut Microtome, yielding sections with a thickness of 50 nm. The samples were analyzed in an FEI Tecnai 12 TEM at an acceleration voltage of 120 kV. The errors reported are the standard deviation.

Electroanalytical Chemistry: All electrochemical studies were carried out with a Gamry 600 potentiostat and data acquisition software (Gamry electrochemistry software version 5.61a) and a three-electrode cell consisting of a silver/silver chloride reference electrode, Pt counter electrode, and then the working electrode of either bare gold, gold modified with SAM, and gold modified with SAM and functionalized with SWCNTs. The electrochemical area was controlled via use of a O-ring with a diameter of 4 mm. Cyclic voltammetry was performed with 1×10^{-3} M solution of ferricyanide in 50×10^{-3} M PBS (0.1 M KCl) from a starting potential of 0.6 V and a switching potential of –0.4 V and an end potential of 0.6 V. Experiments were replicated five times, with the errors reported as standard deviation.

Supporting Information

Supporting Information is available from the Wiley Online Library or from the author.

Acknowledgement

The authors acknowledge financial support of this work by the EPSRC (EP/K027263/1), ERC (Consolidator Grant 614787) and Leverhulme Trust (ECF/2013-306).

Received: December 28, 2015
Revised: February 2, 2016
Published online: February 29, 2016

[1] P. M. Mendes, *Chem. Soc. Rev.* **2013**, *42*, 9207.
[2] F. J. Rawson, C. L. Yeung, S. K. Jackson, P. M. Mendes, *Nano Lett.* **2013**, *13*, 1.
[3] Y. Kim, S. Lee, K. Lee, S. Shim, J. Y. Kim, H. W. Lee, D. Choi, *ACS Appl. Mater. Interfaces* **2014**, *6*, 20423.
[4] F. J. Rawson, D. J. Garrett, D. Leech, A. J. Downard, K. H. R. Baronian, *Biosens. Bioelectron.* **2011**, *26*, 2383.
[5] S. S. Fan, M. G. Chapline, N. R. Franklin, T. W. Tombler, A. M. Cassell, H. J. Dai, *Science* **1999**, *283*, 512.
[6] J. J. Gooding, R. Wibowo, J. Liu, W. Yang, D. Losic, S. Orbons, F. J. Mearns, J. G. Shapter, D. B. Hibbert, *J. Am. Chem. Soc.* **2003**, *125*, 9006.
[7] P. Goldberg-Oppenheimer, T. Hutter, B. A. Chen, J. Robertson, S. Hofmann, S. Mahajan, *J. Phys. Chem. Lett.* **2012**, *3*, 3486.
[8] S. Park, D. W. Park, C. S. Yang, K. R. Kim, J. H. Kwak, H. M. So, C. W. Ahn, B. S. Kim, H. Chang, J. O. Lee, *ACS Nano* **2011**, *5*, 7061.
[9] Z. Liu, Z. Shen, T. Zhu, S. Hou, L. Ying, Z. Shi, Z. Gu, *Langmuir* **2000**, *16*, 3569.
[10] P. Diao, Z. Liu, *Adv. Mater.* **2010**, *22*, 1430.
[11] D. Chattopadhyay, I. Galeska, F. Papadimitrakopoulos, *J. Am. Chem. Soc.* **2001**, *123*, 9451.
[12] Z. Chen, Y. L. Yang, Z. Y. Wu, G. Luo, L. M. Xie, Z. F. Liu, S. J. Ma, W. L. Guo, *J. Phys. Chem. B* **2005**, *109*, 5473.
[13] T. Ferri, D. Frasca, O. A. de Fuentes, R. Santucci, M. Frasconi, *Angew. Chem.-Int. Ed.* **2011**, *50*, 7074.
[14] P. Diao, Z. F. Liu, *J. Phys. Chem. B* **2005**, *109*, 20906.
[15] J. J. Gooding, A. Chou, J. Liu, D. Losic, J. G. Shapter, D. B. Hibbert, *Electrochem. Commun.* **2007**, *9*, 1677.
[16] D. J. Garrett, B. S. Flavel, J. G. Shapter, K. H. R. Baronian, A. J. Downard, *Langmuir* **2010**, *26*, 1848.
[17] J. Yu, D. Losic, M. Marshall, T. Bocking, J. J. Gooding, J. G. Shapter, *Soft Matter* **2006**, *2*, 1081.
[18] B. S. Flavel, J. X. Yu, A. V. Ellis, J. S. Quinton, J. G. Shapter, *Nanotechnology* **2008**, *19*, 12.
[19] F. Patolsky, Y. Weizmann, I. Willner, *Angew. Chem.-Int. Ed.* **2004**, *43*, 2113.
[20] X. L. Nan, Z. N. Gu, Z. F. Liu, *J. Colloid Interface Sci.* **2002**, *245*, 311.
[21] M. S. Jung, S. O. Jung, D. H. Jung, Y. K. Ko, Y. W. Jin, J. Kim, H. T. Jung, *J. Phys. Chem. B* **2005**, *109*, 10584.
[22] H. Y. Wei, S. N. Kim, H. L. Marcus, F. Papadimitrakopoulos, *Chem. Mater.* **2006**, *18*, 1100.
[23] M. W. Marshall, S. Popa-Nita, J. G. Shapter, *Carbon* **2006**, *44*, 1137.
[24] A. Ulman, *Chem. Rev.* **1996**, *96*, 1533.
[25] H. L. Zhang, J. Zhang, H. Y. Li, Z. F. Liu, H. L. Li, *Mater. Sci. Eng. C* **1999**, *8–9*, 179.
[26] J. Liu, A. G. Rinzler, H. J. Dai, J. H. Hafner, R. K. Bradley, P. J. Boul, A. Lu, T. Iverson, K. Shelimov, C. B. Huffman, F. Rodriguez-Macias, Y. S. Shon, T. R. Lee, D. T. Colbert, R. E. Smalley, *Science* **1998**, *280*, 1253.
[27] V. Ganesh, R. R. Pandey, B. D. Malhotra, V. Lakshminarayanan, *J. Electroanal. Chem.* **2008**, *619–620*, 87.
[28] D. A. Tsyboulski, S. M. Bachilo, A. B. Kolomeisky, R. B. Weisman, *ACS Nano* **2008**, *2*, 1770.
[29] R. Duggal, M. Pasquali, *Phys. Rev. Lett.* **2006**, *96*, 4.
[30] J. Gigault, B. Grassl, I. Le Hecho, G. Lespes, *Microchim. Acta* **2011**, *175*, 265.
[31] R. Borsali, R. Pecora, *Soft Matter Characterization*, Springer, Netherlands **2008**.
[32] G. Huber, S. N. Gorb, N. Hosoda, R. Spolenak, E. Arzt, *Acta Biomater.* **2007**, *3*, 607.
[33] B. Zappone, K. J. Rosenberg, J. Israelachvili, *Tribol. Lett.* **2007**, *26*, 191.
[34] B. G. Chen, G. F. Zhong, P. G. Oppenheimer, C. Zhang, H. Tornatzky, S. Esconjauregui, S. Hofmann, J. Robertson, *ACS Appl. Mater. Interfaces* **2015**, *7*, 3626.